



**HAL**  
open science

## **Petrology and bulk chemistry of Yamato-82094, a new type of carbonaceous chondrite**

M. Kimura, Jean-Alix J-A Barrat, M.K. Weisberg, N. Imae, A. Yamaguchi, H. Kojima

► **To cite this version:**

M. Kimura, Jean-Alix J-A Barrat, M.K. Weisberg, N. Imae, A. Yamaguchi, et al.. Petrology and bulk chemistry of Yamato-82094, a new type of carbonaceous chondrite. *Meteoritics and Planetary Science*, 2014, 49 (3), pp.346-357. 10.1111/maps.12254 . insu-00981582

**HAL Id: insu-00981582**

**<https://insu.hal.science/insu-00981582>**

Submitted on 22 Apr 2014

**HAL** is a multi-disciplinary open access archive for the deposit and dissemination of scientific research documents, whether they are published or not. The documents may come from teaching and research institutions in France or abroad, or from public or private research centers.

L'archive ouverte pluridisciplinaire **HAL**, est destinée au dépôt et à la diffusion de documents scientifiques de niveau recherche, publiés ou non, émanant des établissements d'enseignement et de recherche français ou étrangers, des laboratoires publics ou privés.

## Petrology and bulk chemistry of Yamato-82094, a new type of carbonaceous chondrite

M. KIMURA<sup>1,5\*</sup>, J. A. BARRAT<sup>2</sup>, M. K. WEISBERG<sup>3,4</sup>, N. IMAE<sup>5</sup>, A. YAMAGUCHI<sup>5</sup>,  
and H. KOJIMA<sup>5</sup>

<sup>1</sup>Faculty of Science, Ibaraki University, Mito 310-8512, Japan

<sup>2</sup>Université Européenne de Bretagne, 2CNRS UMR 6538 (Domaines Océaniques), U.B.O.-I.U.E.M.,  
Place Nicolas Copernic, Plouzané Cedex 29280, France

<sup>3</sup>Department of Physical Sciences, Kingsborough College and Graduate School of the City University of New York,  
Brooklyn, New York 11235, USA

<sup>4</sup>Department of Earth and Planetary Sciences, American Museum of Natural History, New York, New York 10024, USA

<sup>5</sup>National Institute of Polar Research, Tokyo 190-8518, Japan

\*Corresponding author. E-mail: makotoki@mx.ibaraki.ac.jp

(Received 04 April 2013; revision accepted 18 November 2013)

---

**Abstract**—Carbonaceous chondrites are classified into several groups. However, some are ungrouped. We studied one such ungrouped chondrite, Y-82094, previously classified as a CO. In this chondrite, chondrules occupy 78 vol%, and the matrix is distinctly poor in abundance (11 vol%), compared with CO and other C chondrites. The average chondrule size is 0.33 mm, different from that in C chondrites. Although these features are similar to those in ordinary chondrites, Y-82094 contains 3 vol% Ca-Al-rich inclusions and 5% amoeboid olivine aggregates (AOAs). Also, the bulk composition resembles that of CO chondrites, except for the volatile elements, which are highly depleted. The oxygen isotopic composition of Y-82094 is within the range of CO and CV chondrites. Therefore, Y-82094 is an ungrouped C chondrite, not similar to any other C chondrite previously reported. Thin FeO-rich rims on AOA olivine and the mode of occurrence of Ni-rich metal in the chondrules indicate that Y-82094 is petrologic type 3.2. The extremely low abundance of type II chondrules and high abundance of Fe-Ni metal in the chondrules suggest reducing condition during chondrule formation. The depletion of volatile elements indicates that the components formed under high-temperature conditions, and accreted to the parent body of Y-82094. Our study suggests a wider range of formation conditions than currently recorded by the major C chondrite groups. Additionally, Y-82094 may represent a new, previously unsampled, asteroidal body.

---

### INTRODUCTION

Carbonaceous chondrites (C chondrites, hereafter) are among the most primitive materials in the solar system, and are classified into eight major chemical groups: CI, CM, CO, CV, CR, CH, CB, and CK (e.g., Weisberg et al. 2006). The groups are distinguished from one another by petrographic features, constituent components, mineralogy, and chemical and isotopic compositions. However, some C chondrites, such as Acfer 094 (Newton et al. 1995), cannot be classified into any of the known groups, and are distinguished by their

unusual features (e.g., Brearley and Jones 1998; Weisberg et al. 2006). Such ungrouped chondrites are important not only for classification, but to extend the range material known in the asteroid belt and to explore the range of formation conditions in the early solar system.

Herein, we present a study of the Yamato (Y)-82094 ungrouped C chondrite. Originally it was classified as a CO chondrite (Yanai and Kojima 1987). Sears et al. (1991) classified it as a CO 3.5 by thermoluminescence. However, Scott et al. (1992) suggested that the texture of Y-82094 is different from

that of most CO chondrites. Later, Imae and Kojima (2000) described the unusual features in Y-82094; larger average diameter of chondrules than that of COs, lower FeO content in its bulk composition, and a higher abundance of Fe-Ni metal. Therefore, they suggested that Y-82094 is an unusual CO chondrite.

Here, we report the petrography, mineralogy, and bulk chemistry of this unusual chondrite, to explore its characteristic features, classification, and formation conditions. We conclude that Y-82094 is an ungrouped C chondrite. As it preserves characteristics that distinguish it from the other known C chondrites, Y-82094 sheds light on the diversity of formation conditions for C chondrite groups. Preliminary results were reported by Kimura et al. (2012).

## SAMPLES AND EXPERIMENTAL METHODS

The original (recovered) weight of Y-82094 was 216.59 g. We investigated five polished thin sections, 91-1, 91-4, 96-1, 96-2, and 111-1, from this sample.

Backscattered electron (BSE) images were obtained using the JEOL JSM5900LV scanning electron microscope at the National Institute of Polar Research (NIPR), and the Hitachi S4700 Field Emission Gun scanning electron microscope at the American Museum of Natural History. Mineral analyses were obtained using the JEOL JXA8200 electron-probe microanalyzer at NIPR, with a focused (approximately 1  $\mu\text{m}$ ) beam and 10 nA beam current. The matrix was measured by using a defocused beam (5  $\mu\text{m}$  in diameter) for random 228 points to avoid opaque minerals, and an average bulk matrix composition was calculated. The elemental X-ray map of the section was obtained using the Cameca SX100 electron-probe microanalyzer at the American Museum of Natural History. All these analytical methods were the same as those by Yamaguchi et al. (2011) and Weisberg et al. (2011).

The modal composition was determined from X-ray and BSE maps of the whole area of one thin section, Y-82094, 91-1, 188.6 mm<sup>2</sup>. ImageJ software was used to calculate the mode, based on the X-ray intensities of each pixel. We identified some phases using a laser micro Raman spectrometer (JASCO NRS 1000) at the NIPR, after the method of Yamaguchi et al. (2011).

Major and trace element abundances were determined, respectively, by inductively coupled plasma atomic emission spectrometry (ICP-AES) and inductively coupled plasma sector field mass spectrometry (ICP-SFMS) using the same procedure as Barrat et al. (2012). The precision and accuracy of the results were estimated using well-characterized standards and sample duplicates. For ICP-AES results, the accuracy is better than 7% for Na and P, and

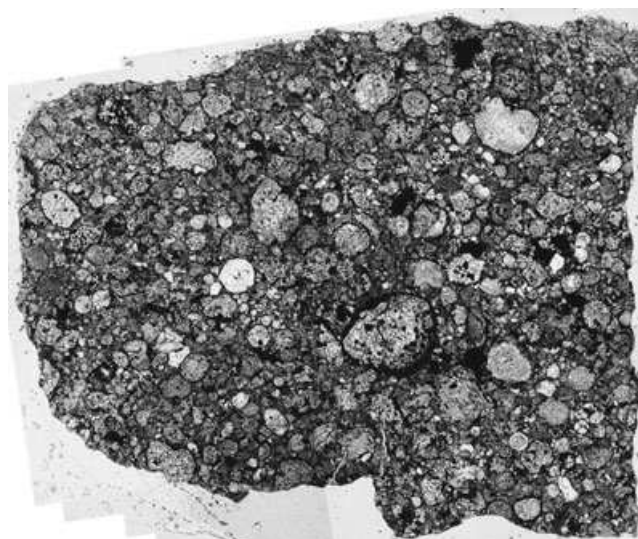


Fig. 1. Photomicrograph (transmitted light) of a section of Y-82094 (91-4). The texture is typical of unequilibrated chondrites, consisting of sharply delineated chondrules and low abundance of matrix. Width of image is 15 mm.

probably much better than 3% for the other elements. For ICP-SFMS, the accuracy is better than 9% for W, 4% for Pb, and less than 3% for the other elements.

## RESULTS

### Petrography

#### Overall Features

Y-82094 shows a typical chondritic texture, dominated by spherical chondrules and their fragments (Fig. 1). One of the distinct features of Y-82094 is its low abundance of opaque matrix (Figs. 1 and 2). The matrix modal abundance is only 11 vol% (Table 1), whereas chondrules and fragments occupy 78 vol%. Table 1 also summarizes the modal abundances of Y-82094 and other anhydrous chondrites. The chondrule abundance in Y-82094 is much higher than that in C and R chondrites. On the other hand, the matrix abundance in Y-82094 is much lower than in C and R chondrites, except for CH chondrites. The high abundance of chondrules and low abundance of the matrix in Y-82094 are within the range of chondrule and matrix abundances in unequilibrated O chondrites (Table 1).

On the other hand, Figs. 2 and 3 show the occurrence of irregular-shaped refractory inclusions, a Ca-Al-rich inclusion (CAI), and an amoeboid olivine aggregate (AOA), which are similar to inclusions that are common in C chondrites and rare in O chondrites. CAIs and AOAs are abundantly distributed throughout Y-82094, making up 3 and 5 vol%, respectively (Fig. 3).

Table 1. Modal abundances (vol%) of components in Y-82094 compared with data from other chondrite groups.

|         | Chondrule         | Matrix  | Refractory inclusion | Metal (outside chondrule) |
|---------|-------------------|---------|----------------------|---------------------------|
| Y-82094 | 78.1 <sup>a</sup> | 11.1    | 8.2 <sup>b</sup>     | 2.6 <sup>c</sup>          |
| CO      | 48                | 34      | 13                   | 1–5                       |
| CV      | 45                | 40      | 10                   | 0–5                       |
| CR      | 50–60             | 30–50   | 0.5                  | 5–8                       |
| CH      | ~70               | 5       | 0.1                  | 20                        |
| H-L-LL  | 60–80             | 10–15   | ≪1                   | 2–10                      |
| R       | 35–50             | 42 ± 11 | ≪1                   | 0.1                       |
| EH-EL   | 60–80             | 8–10    | ≪1                   | 8–15                      |

Chondrite data: after Brearley and Jones (1998), Weisberg et al. (2006), Rubin (2010), and Bischoff et al. (2011).

<sup>a</sup>Including opaque minerals (6.9% Fe-Ni metal and 0.6 troilite).

<sup>b</sup>3.0% Ca-Al-rich inclusions and 5.2% amoeboid olivine aggregates.

<sup>c</sup>1.2% Fe-Ni metal and 1.4 sulfides.

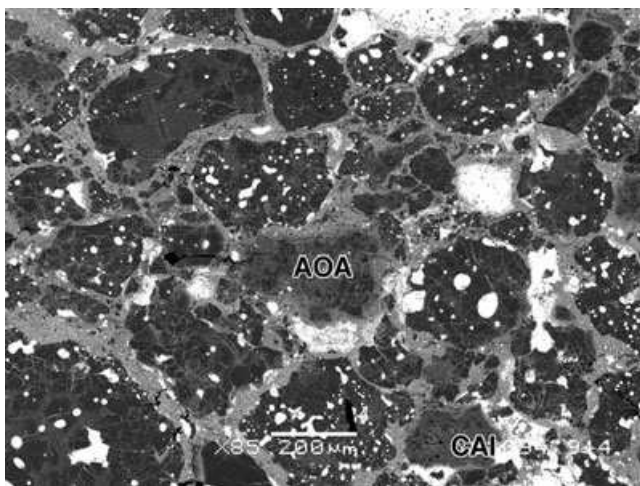


Fig. 2. Backscattered electron (BSE) image of Y-82094 (91-4) showing refractory inclusions (amoeboid olivine aggregate: AOA and Ca-Al-rich inclusion: CAI) among the numerous chondrules and matrix. Chondrules are dominantly type I and contain variable amounts of Fe-Ni (white). Also, note that the matrix abundance is low compared with most other C chondrites.

The shock degree of Y-82094 is S2 (Scott et al. 1992). Impact-induced shock veins, melt pocket, brecciated texture, and high-pressure minerals are not present.

### Chondrules

Sharply delineated, spherical chondrules are the most abundant component in Y-82094. Table 2 summarizes the characteristic features of the chondrules. Their apparent average diameter is 0.33 mm ( $\sigma = 0.19$ ) after the measurement for 651 chondrules. Chondrules in Y-82094 are not surrounded by coarse-grained igneous rims like those in CO chondrites (Rubin 2010).

The abundances of porphyritic, barred, and nonporphyritic (radial and cryptocrystalline) chondrules

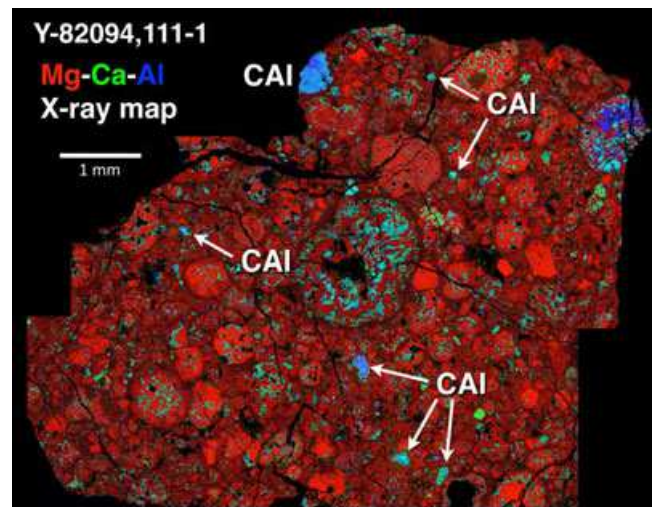


Fig. 3. Combined elemental (Mg-Ca-Al) composition map for the section of Y-82094 (111-1). Ca-Al-rich inclusions (CAIs), especially enriched in Al, are common in the section.

are 97.5, 2.1, and 0.4% of all chondrules, respectively (Table 2; Fig. 2). Type II chondrules are rare in Y-82094 (0.9%) (Table 2). One of the type II chondrules studied contains a magnesian relic olivine within a ferroan olivine phenocryst (Fig. 4).

Most porphyritic chondrules consist of olivine and Ca-poor pyroxene (mostly clinoenstatite), with minor amounts of Ca-rich pyroxene, plagioclase, and spinel group minerals. Silica grains, less than 10  $\mu\text{m}$ , are also present as anhedral crystals in the mesostases of the abundant type I chondrules. Silica is generally rare in chondrules in other C chondrites. In abundant chondrules, the mesostasis is weakly devitrified, which consists of a fine-grained intergrowth of  $\mu\text{m}$ -sized plagioclase and Ca-pyroxene, occasionally with a silica mineral. Some porphyritic chondrules appear to contain a glassy mesostasis, based on optical properties. However, such mesostasis also contains plagioclase and

Table 2. Petrographic features of chondrules in Y-82094 compared with data from other chondrite groups.

|         | Diameter (mm) | Texture (%) |        |        | Type (%) |         |
|---------|---------------|-------------|--------|--------|----------|---------|
|         |               | Porphyritic | Barred | RP + C | Type I   | Type II |
| Y-82094 | 0.33          | 97.5        | 2.1    | 0.4    | 99.1     | 0.9     |
| CO      | 0.15          | 95          | 2      | 3      | 90       | 10      |
| CV      | 1.0           | 94          | 6      | 0.3    | 95       | 5       |
| H-L-LL  | 0.3–0.6       | 84          | 4      | 11     | 20–30    | 70–80   |

Chondrite data: after Jones (2012).

RP = radial pyroxene; C = cryptocrystalline chondrule.

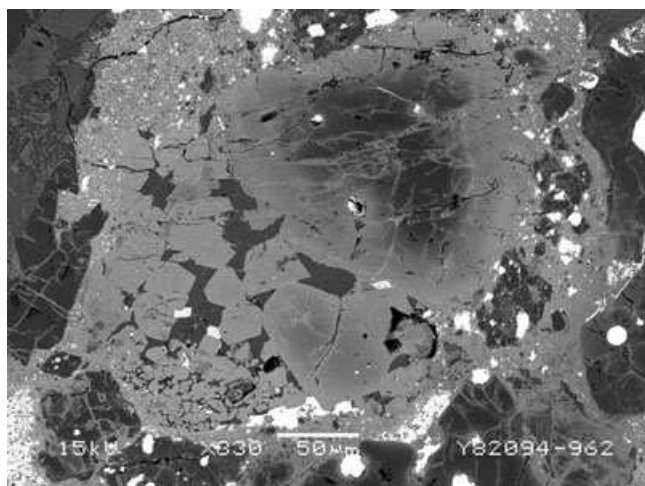


Fig. 4. Backscattered electron image of a type II chondrule in Y-82094 (91-1). It mainly consists of ferroan olivine phenocrysts, mesostasis (dark gray), and chromite (white). The large phenocryst contains a magnesian “relic” forsteritic olivine grain.

Ca-pyroxene of submicron-size, as determined from Raman analysis. In rare cases, nepheline, below 10  $\mu\text{m}$ , replaces plagioclase.

About 70% of the type I chondrules in Y-82094 contain abundant Fe-Ni metal spherules (10–40 vol% of the chondrule) (Fig. 2), whereas troilite is mostly absent within the chondrules, but present in the peripheral rims of chondrules. Chromite occurs in the rare type II chondrules.

### Refractory Inclusions

Refractory inclusions are abundant in Y-82094, and can be divided into CAIs and AOAs. Many CAIs are complete, unfractured objects surrounded by rims, consisting mainly of Ca-rich pyroxene. The sizes of CAIs range from 80 to 1000  $\mu\text{m}$  (340  $\mu\text{m}$  on average).

Most CAIs (approximately 65% of the total number of CAIs) consist of melilite (Geh<sub>61-99</sub>), spinel, and Ca-rich pyroxene (Fig. 5), with perovskite, and can be classified as type A inclusions. Other common CAIs

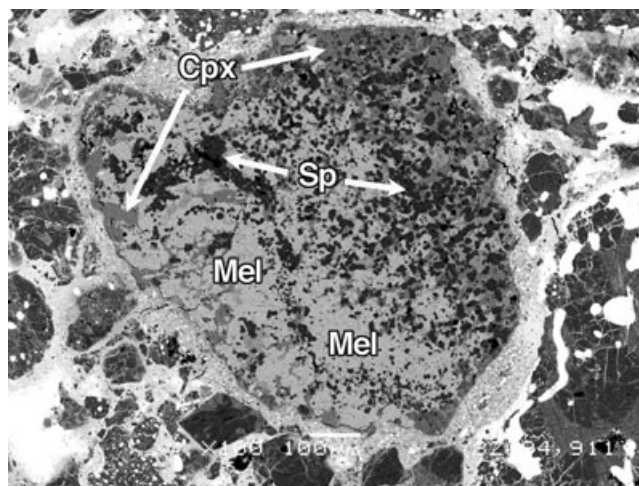


Fig. 5. Backscattered electron image of a melilite (Mel)-rich inclusion in Y-82094 (91-1). This inclusion also contains spinel (Sp) and Ca-rich pyroxene (Cpx).

mainly consist of spinel and Ca-rich pyroxene. These are spinel-pyroxene inclusions and make up 23% of the total number of CAIs. Rare CAIs containing anorthite, hibonite, and grossite are also present. Fe-Ni metal is rarely encountered in CAIs. Secondary alteration minerals, such as ilmenite, nepheline, and sodalite, are quite rare in the CAIs from Y-82094. Secondary Ca-rich phases, such as hedenbergite and andradite, were not found.

Amoeboid olivine aggregates are also common in Y-82094. They are 90–730  $\mu\text{m}$  (290  $\mu\text{m}$  in average) in size. The average size distribution is within the range of AOAs in CO chondrites, 150–440  $\mu\text{m}$  (Rubin 1998). The AOAs mostly consist of forsteritic olivine, with minor amounts of interstitial anorthite and Ca-rich pyroxene (Fig. 6). The AOA olivine generally has thin FeO-rich rims, less than 3  $\mu\text{m}$  in width. Melilite, spinel, and Ca-poor pyroxene are often present in the AOAs. In rare cases, Ca-poor pyroxene is present in the peripheral parts of AOAs, as observed by Krot et al. (2004) in AOAs from CVs and other C chondrites. Tiny grains of Fe-Ni metal,  $\leq 10$   $\mu\text{m}$ , are present in many of the AOAs.

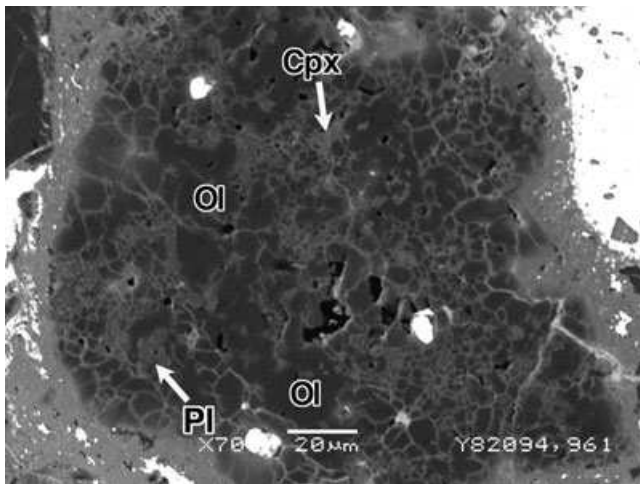


Fig. 6. Backscattered electron image of an amoeboid olivine aggregate (AOA), consisting of forsteritic olivine (Ol) with interstitial plagioclase (Pl) and Ca-pyroxene (Cpx) in Y-82094 (96-1). The forsterites are surrounded by very thin ferroan rims.

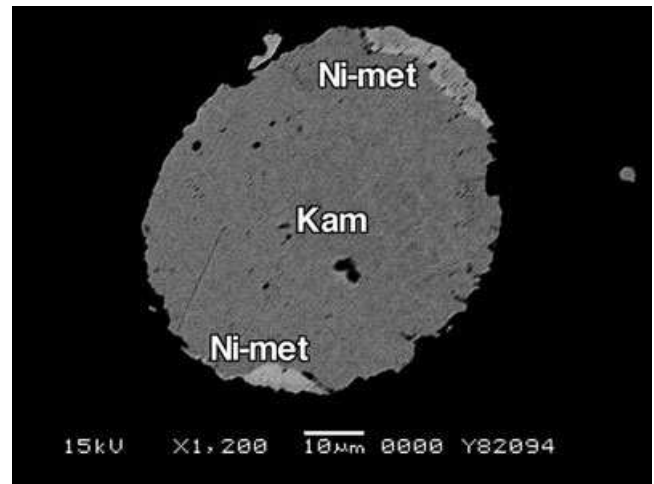


Fig. 7. Backscattered electron image of a metal spherule in a chondrule of Y-82094 (91-1). It consists of kamacite (Kam) with Ni-rich metal (Ni-met).

### Fe-Ni Metal and Sulfide Minerals

The total abundance of Fe-Ni metal and sulfide (mostly troilite, as described below) is 10.1 vol%. However, the abundance of Fe-Ni metal (8.1 vol%) is much higher than that of troilite (2.0%).

Fe-Ni metal occurs in the interiors and on surfaces of chondrules and AOAs, and as isolated grains in the matrix, as documented by Shibata and Matsueda (1994). Such occurrences are the same as in CO chondrites (Kimura et al. 2008). Considering the total metal abundance of 8.1 vol%, 6.9% is associated with chondrules and 1.2% occurs as isolated grains. High abundances of Fe-Ni metal in chondrules are another characteristic feature of Y-82094. In chondrule interiors, Fe-Ni metal typically shows spherical form and consists of kamacite or kamacite with Ni-rich metal (several to several tens of  $\mu\text{m}$  in size) (Fig. 7).

Troilite typically occurs as isolated minerals, especially surrounding Fe-Ni metal, and generally shows a porous texture. Rare pentlandite is present in association with isolated troilite grains.

### Matrix

Figure 8 shows a matrix area. The matrix mainly consists of ferroan olivine, and shows a sintered texture. The olivine grain boundaries are not well distinguished. The matrix also contains tiny fragmental grains, below 10  $\mu\text{m}$ , of forsteritic olivine, Ca-poor and -rich pyroxene, a Na-rich feldspathic mineral, phosphate, and Fe-Ni metal. No phyllosilicates were found.

Table 3 and Fig. 9 show the composition of the matrix, which plots along the forsterite-fayalite tie line.

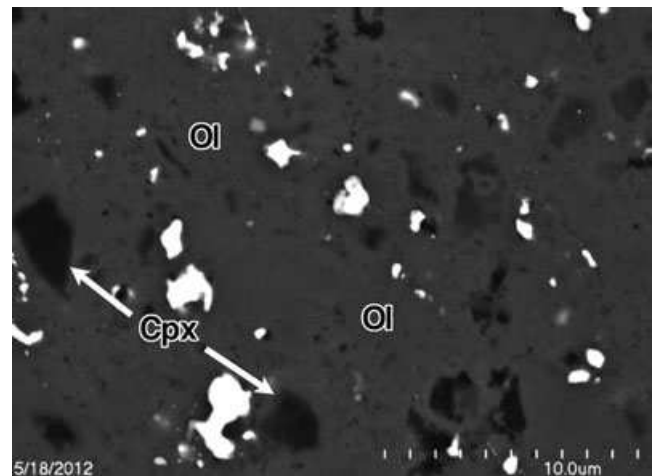


Fig. 8. Backscattered electron image of a matrix area in Y-82094 (111-1). The dominant phase is olivine, showing a sintered texture, with minor Ca-rich pyroxene (Cpx). Bright grains are mostly Fe-Ni metal.

This indicates that ferroan olivine is the major component of the matrix with minor  $\text{Al}_2\text{O}_3$  (1.8 wt%), CaO (0.9), and  $\text{Na}_2\text{O}$  (0.3), suggesting the presence of other minor components.

### Mineralogy

#### Olivine

Table 3 shows selected analyses of the constituent phases. Olivine is common in chondrules and their fragments, AOAs, and matrix. Olivine in type I and II chondrules is  $\text{Fo}_{89-99}$  and  $\text{Fo}_{58-82}$ , respectively. One of the type II chondrules studied contains a relic forsterite

Table 3. Representative compositions of minerals and the average matrix composition in Y-82094.

| Occurrence          | Type | Mineral               | SiO <sub>2</sub> | TiO <sub>2</sub> | Al <sub>2</sub> O <sub>3</sub> | Cr <sub>2</sub> O <sub>3</sub> | FeO  | MnO  | MgO  | CaO  | Na <sub>2</sub> O | K <sub>2</sub> O | Total | Fo   | En   | Fs   | Wo   | An   | Ab   | Or  |
|---------------------|------|-----------------------|------------------|------------------|--------------------------------|--------------------------------|------|------|------|------|-------------------|------------------|-------|------|------|------|------|------|------|-----|
| Chondrule           | I    | Olivine               | 41.7             | b.d.             | b.d.                           | 0.15                           | 1.2  | b.d. | 56.4 | 0.35 | b.d.              | b.d.             | 99.8  | 98.4 |      |      |      |      |      |     |
| Chondrule           | I    | Olivine               | 41.7             | 0.06             | 0.08                           | b.d.                           | 4.8  | 0.09 | 53.3 | 0.24 | b.d.              | b.d.             | 100.3 | 94.9 |      |      |      |      |      |     |
| Chondrule           | II   | Olivine               | 36.9             | b.d.             | 0.07                           | 0.17                           | 32.0 | 0.38 | 31.1 | 0.14 | 0.04              | b.d.             | 100.8 | 63.3 |      |      |      |      |      |     |
| Chondrule           | II   | Olivine               | 41.9             | b.d.             | 0.05                           | 0.12                           | 2.2  | b.d. | 54.7 | 0.14 | b.d.              | b.d.             | 99.0  | 97.7 |      |      |      |      |      |     |
| AOA                 |      | Olivine               | 42.8             | b.d.             | 0.04                           | b.d.                           | 0.20 | 0.08 | 57.2 | 0.25 | b.d.              | b.d.             | 100.6 | 99.5 |      |      |      |      |      |     |
| AOA                 |      | Olivine               | 41.5             | b.d.             | b.d.                           | b.d.                           | 5.6  | b.d. | 52.6 | 0.14 | b.d.              | b.d.             | 99.8  | 94.2 |      |      |      |      |      |     |
| Chondrule           | I    | Ca-poor pyroxene      | 58.7             | 0.04             | 0.32                           | 0.53                           | 1.7  | 0.30 | 37.7 | 0.29 | b.d.              | b.d.             | 99.6  |      | 97.0 | 2.5  | 0.5  |      |      |     |
| Chondrule           | II   | Ca-poor pyroxene      | 56.5             | 0.04             | 0.17                           | 0.87                           | 7.9  | 0.41 | 32.1 | 0.90 | 0.05              | b.d.             | 99.0  |      | 86.3 | 12.0 | 1.8  |      |      |     |
| AOA                 |      | Ca-poor pyroxene      | 58.5             | 0.06             | 0.28                           | 0.16                           | 0.91 | b.d. | 38.0 | 0.55 | 0.07              | b.d.             | 98.5  |      | 97.7 | 1.3  | 1.0  |      |      |     |
| Chondrule           | I    | Ca-rich pyroxene      | 55.6             | 0.40             | 1.1                            | 0.50                           | 0.16 | 0.15 | 22.9 | 18.6 | b.d.              | b.d.             | 99.4  |      | 63.0 | 0.3  | 36.8 |      |      |     |
| AOA                 |      | Ca-rich pyroxene      | 29.7             | 14.0             | 22.8                           | 0.10                           | 0.13 | b.d. | 9.4  | 23.3 | 0.06              | b.d.             | 99.8  |      |      |      |      |      |      |     |
| CAI                 |      | Ca-rich pyroxene      | 37.8             | 6.2              | 21.0                           | 0.19                           | 0.05 | b.d. | 9.6  | 25.2 | b.d.              | b.d.             | 100.1 |      |      |      |      |      |      |     |
| Chondrule           | I    | Plagioclase           | 48.9             | 0.10             | 32.5                           | b.d.                           | 0.57 | b.d. | 0.14 | 15.7 | 2.3               | b.d.             | 100.1 |      |      |      |      | 79.1 | 20.7 | 0.2 |
| Chondrule           | II   | Plagioclase           | 55.9             | 0.06             | 27.7                           | b.d.                           | 0.78 | b.d. | 0.33 | 10.3 | 5.4               | 0.05             | 100.5 |      |      |      |      | 51.2 | 48.8 | 0.0 |
| AOA                 |      | Plagioclase           | 42.6             | 0.05             | 36.3                           | b.d.                           | 0.17 | 0.17 | 0.38 | 19.8 | 0.07              | b.d.             | 99.6  |      |      |      |      | 99.3 | 0.6  | 0.1 |
| CAI                 |      | Plagioclase           | 43.1             | 0.04             | 36.1                           | b.d.                           | 0.15 | b.d. | b.d. | 20.4 | 0.06              | b.d.             | 99.8  |      |      |      |      | 99.5 | 0.5  | 0.0 |
| CAI                 |      | Melilite              | 22.5             | 0.05             | 36.0                           | b.d.                           | 0.04 | b.d. | 0.40 | 41.1 | b.d.              | b.d.             | 100.1 |      |      |      |      |      |      |     |
| Chondrule           | I    | Silica                | 99.9             | b.d.             | 0.13                           | b.d.                           | 0.08 | b.d. | 0.07 | b.d. | 0.12              | b.d.             | 100.3 |      |      |      |      |      |      |     |
| Chondrule           | I    | Spinel <sup>a</sup>   | 0.10             | 0.32             | 70.7                           | 0.24                           | 2.6  | b.d. | 26.0 | 0.06 | b.d.              | b.d.             | 100.2 |      |      |      |      |      |      |     |
| Chondrule           | II   | Chromite <sup>b</sup> | 0.28             | 1.1              | 0.06                           | 62.2                           | 30.5 | 0.40 | 1.6  | 0.07 | 0.06              | b.d.             | 97.1  |      |      |      |      |      |      |     |
| AOA                 |      | Spinel                | 0.07             | 0.11             | 71.5                           | 0.21                           | 0.57 | b.d. | 27.9 | 0.09 | b.d.              | b.d.             | 100.5 |      |      |      |      |      |      |     |
| CAI                 |      | Spinel                | 0.06             | 0.21             | 70.8                           | 0.18                           | 0.13 | b.d. | 27.6 | 0.10 | b.d.              | b.d.             | 99.0  |      |      |      |      |      |      |     |
| Chondrule           | I    | Mesostasis            | 56.5             | 0.17             | 23.7                           | 0.13                           | 0.15 | b.d. | 3.2  | 14.4 | 1.7               | b.d.             | 100.0 |      |      |      |      |      |      |     |
| Chondrule           | II   | Mesostasis            | 60.0             | 0.47             | 20.6                           | 0.08                           | 3.2  | 0.17 | 2.3  | 6.3  | 7.4               | 0.05             | 100.6 |      |      |      |      |      |      |     |
| Matrix <sup>c</sup> |      |                       | 32.6             | 0.07             | 1.8                            | 0.53                           | 36.2 | 0.36 | 24.1 | 0.90 | 0.27              | b.d.             | 98.0  |      |      |      |      |      |      |     |

b.d. = below detection limits (3 $\sigma$ ); 0.03 for SiO<sub>2</sub>, Al<sub>2</sub>O<sub>3</sub>, MgO, and CaO; 0.04 for TiO<sub>2</sub>, Na<sub>2</sub>O, and K<sub>2</sub>O; 0.08 for MnO; and 0.10 for Cr<sub>2</sub>O<sub>3</sub>.

<sup>a</sup>Also containing 0.20% V<sub>2</sub>O<sub>5</sub>.

<sup>b</sup>Also containing 0.64% V<sub>2</sub>O<sub>5</sub> and 0.22 ZnO.

<sup>c</sup>Matrix data were averaged composition, and contain 1.1% NiO.

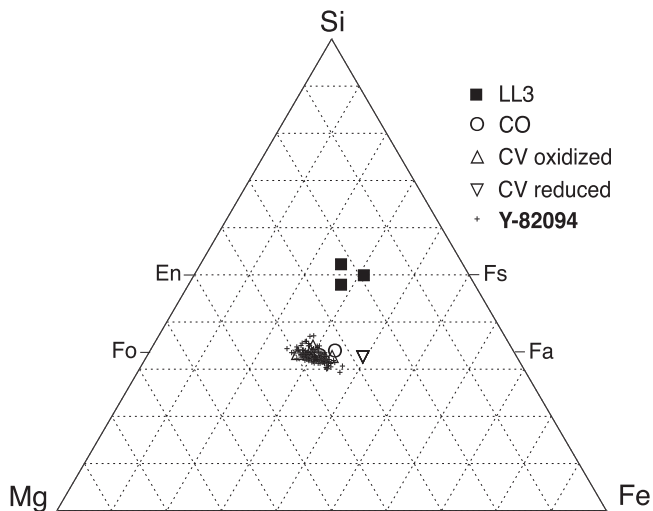


Fig. 9. Matrix compositions of Y-82094 in atomic Si-Mg-Fe plot, compared with those in LL3 (Huss et al. 1981; Ikeda et al. 1981), and CO and CV chondrites (Zolensky et al. 1993). The composition of the matrix in Y-82094 is similar to that in CO and CV chondrites, and different from that in LL3 chondrites.

grain (e.g.,  $\text{Fo}_{99}$ ). The average  $\text{Cr}_2\text{O}_3$  content and standard deviation for FeO-bearing olivine grains ( $>2$  wt% FeO) are 0.11 and 0.07, respectively.

Olivine in AOAs is mostly  $>\text{Fo}_{96}$ . The peripheral rims of the olivine grains in AOAs are too thin to be precisely measured. However, the olivine generally becomes more ferroan close to the rims ( $\text{Fo}_{71-94}$ ).

### Pyroxene

Pyroxene is the second most abundant mineral in Y-82094. It is divided into Ca-poor ( $<0.15$  atomic Ca/(Ca + Mg + Fe) ratio) and Ca-rich pyroxenes. Ca-poor pyroxenes are abundant in type I chondrites, and are magnesian ( $\text{En}_{85-99}\text{Fs}_{0.3-6}\text{Wo}_{0.2-14}$ ). On the other hand, Ca-poor pyroxene is rare in type II chondrites and is ferroan ( $\text{En}_{64-86}\text{Fs}_{12-24}\text{Wo}_{0.4-14}$ ). Ca-poor pyroxene also occurs in the peripheral parts of AOAs, and in this textural setting, it is always magnesian ( $\text{En}_{95-98}\text{Fs}_{1-2}\text{Wo}_{1-2}$ ).

Ca-rich pyroxene is present in chondrules as a mesostasis phase and often as phenocrysts, and occurs in AOAs, and CAIs. In chondrules, the Ca-pyroxene is  $\text{En}_{53-73}\text{Fs}_{0.2-4}\text{Wo}_{26-47}$  in type I and  $\text{En}_{31-47}\text{Fs}_{15-23}\text{Wo}_{34-46}$  in type II chondrules. Ca-rich pyroxenes in chondrules contain 1.0–8.4 wt%  $\text{Al}_2\text{O}_3$ , and 0.3–2.9  $\text{TiO}_2$ . On the other hand, Ca-rich pyroxenes are enriched in  $\text{Al}_2\text{O}_3$  0.9–29.5 wt% in CAIs, and 0.4–23.4 in AOAs. The  $\text{TiO}_2$  contents of the Ca-pyroxene in CAIs and AOAs are also high, up to 15.2 wt% and 14.0, respectively.

### Plagioclase and Mesostasis

Plagioclase ( $\text{An}_{76-98}\text{Ab}_{2-24}\text{Or}_{0-0.4}$ ) in type I chondrules is anorthitic, whereas in type II chondrules, the plagioclase is enriched in Na ( $\text{An}_{34-54}\text{Ab}_{45-66}\text{Or}_{0-3}$ ). Highly Ca-rich plagioclase ( $\text{An}_{98-100}$ ) is a common mineral in CAIs and AOAs.

As mentioned before, the mesostasis in chondrules consists of a fine-grained intergrowth of plagioclase and Ca-pyroxene, which cannot be individually measured. However, the mesostasis in type I chondrules is enriched in CaO, whereas that in type II contains a high abundance of  $\text{Na}_2\text{O}$  (Table 3), which is consistent with the compositions of plagioclases in these chondrules.

### Silica Minerals

Silica minerals often occur within the mesostases of chondrules. They show Raman peaks at 418 and  $226\text{ cm}^{-1}$ , indicative of cristobalite. They contain 0.1–0.8 wt%  $\text{Al}_2\text{O}_3$  and  $<0.4$   $\text{Na}_2\text{O}$ .

### Spinel Group Minerals

Spinel group minerals are divided into spinel and chromite. Spinel occurs in nearly all refractory inclusions and in many type I chondrules, whereas chromites are encountered only in type II chondrules. Such occurrences are consistent with those in unequilibrated O chondrites (Kimura et al. 2006). The atomic Mg/(Mg + Fe) ratios of spinels range 0.53–1.00 for refractory inclusions, and 0.70–0.99 for type I chondrules. The Al/(Al + Cr) ratios are 0.98–1.00 for inclusions, and 0.97–1.00 for type I chondrules. The  $\text{TiO}_2$ ,  $\text{V}_2\text{O}_3$ , and ZnO contents are  $<0.6$  and 0.2–0.4 wt%,  $<0.7$  and 0.1–0.3, and  $<0.3$  and  $<0.4$ , in inclusions and type I chondrules, respectively.

The atomic Mg/(Mg + Fe) and Al/(Al + Cr) ratios of chromites are 0.08–0.21 and 0–0.43, and they contain 0.9–1.2 wt%  $\text{TiO}_2$ , 0.6–0.7  $\text{V}_2\text{O}_3$ , and 0.1–0.4 ZnO, respectively.

### Fe-Ni Metal and Sulfides

The chemical composition of Fe-Ni metal in Y-82094 was reported by Shibata and Matsueda (1994) and Imae and Kojima (2000) and our results are consistent with theirs. Here, we briefly report our results. After Kimura et al. (2008), we call all Fe-Ni metal with  $<7.5$  wt% Ni “kamacite,” and all other metal is referred to as “Ni-rich metal.” Kamacite and Ni-rich metal contain 0.3–1.0 and 0.1–0.6 wt% Co, and 5.2–7.3 and 15–48 Ni, respectively. Kamacite is more enriched in Co than Ni-rich metal. Both metals contain  $<0.1$  wt% Si,  $<0.1$  P, and  $<0.5$  Cr. Kamacite is slightly enriched in Ni, in comparison with metal in CO chondrites, as shown by Shibata and Matsueda (1994).

Table 4. Major and trace element abundances for Yamato-82094 (oxides in wt% and other elements in  $\mu\text{g g}^{-1}$ ).

| ICP-AES                                | ICP-SFMS    | ICP-SFMS    | ICP-SFMS    | ICP-SFMS    |
|--|-------------|-------------|-------------|-------------|
| TiO <sub>2</sub> (0.14)                | Li (1.71)   | Ga (4.13)   | Nd (0.863)  | Hf (0.185)  |
| Al <sub>2</sub> O <sub>3</sub> (2.96)  | Be (0.0371) | Rb (0.375)  | Sm (0.279)  | Ta (0.0268) |
| FeO (32.55)                            | P (1044)    | Sr (13.56)  | Eu (0.106)  | W (0.18)    |
| MnO (0.16)                             | K (159)     | Y (2.74)    | Gd (0.364)  | Pb (0.05)   |
| MgO (26.5)                             | Sc (10)     | Zr (6.12)   | Tb (0.0675) | Th (0.0512) |
| CaO (2.41)                             | Ti (733)    | Nb (0.479)  | Dy (0.455)  | U (0.0129)  |
| Na <sub>2</sub> O (0.46)               | V (82.1)    | Cs (0.0297) | Ho (0.0984) |             |
| P <sub>2</sub> O <sub>5</sub> (0.3)    | Mn (1133)   | Ba (4.49)   | Er (0.287)  |             |
| Cr <sub>2</sub> O <sub>3</sub> (0.508) | Co (635)    | La (0.431)  | Tm (0.0473) |             |
| Co (805)                               | Cu (90.8)   | Ce (1.08)   | Yb (0.299)  |             |
| Ni (16000)                             | Zn (81.5)   | Pr (0.169)  | Lu (0.0429) |             |

ICP-AES = inductively coupled plasma atomic emission spectrometry; ICP-SFMS = inductively coupled plasma sector field mass spectrometry.

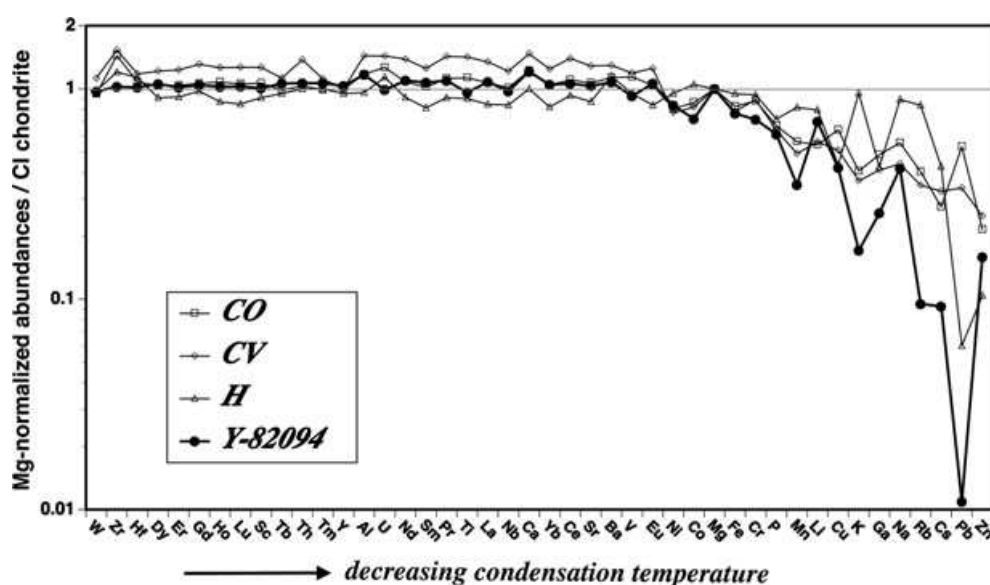


Fig. 10. Diagram showing the Mg- and CI-normalized bulk composition of Y-82094, compared with that of CO, CV, and H chondrites (Wasson and Kallemeyn 1988). The CI chondrite data are after Barrat et al. (2012).

Troilite has Ni and Cu contents below detection limits (0.03 wt%). Pentlandite contains 14–17 wt% Ni and <0.1 Co.

### Bulk Chemistry

Table 4 shows the bulk chemical composition of Y-82094. Figure 10 is the diagram of the Mg- and CI-normalized bulk composition, compared with the other chondrites. The elements are plotted with decreasing condensation temperature. The abundance pattern of refractory elements, especially from W to Eu, including REEs, is almost flat. This is close to CO and CI chondrite abundances, which are lower and higher than those of CV and H chondrite, respectively. However, some elements, such as Zr, Ti, and V, in

Y-82094 are slightly depleted compared with those of CO chondrites. On the other hand, volatile elements (Mn to Zn) decrease with decreasing condensation temperature, and are evidently depleted, compared with the other chondrites. K, Rb, Cs, and Pb are particularly highly depleted.

## DISCUSSION

### Classification of Chemical Group

Y-82094 was originally classified as a CO chondrite. However, this study shows that Y-82094 has features partly similar to those of both CO and O chondrites, but also has some unique characteristics different from the other chondrites. Here, we summarize the

characteristic features, and then discuss the classification (i.e., chemical group) of Y-82094.

The modal abundances of components in Y-82094 are similar to those in O chondrites, especially the high-chondrule and low-matrix abundance. The apparent average diameter of chondrules, 0.33 mm, is intermediate between those in CO and CV, and different from those in any other C chondrite group (Jones 2012). The variations of modal abundances and size distribution of chondrules in CO chondrites are narrow (McSween 1977a; Rubin 1989, 1998), and the mode and chondrule sizes of Y-82094 are well outside the CO range. On the other hand, the chondrule size is within the range of that in unequilibrated O chondrites. The chondrule size in R chondrites (0.4 mm after Bischoff et al. 2011) is also similar to that in Y-82094, although the modal abundance and oxygen isotopic composition, as mentioned later, are evidently different from those in Y-82094.

However, Y-82094 also contains a high abundance of refractory inclusions (8 vol%). This is a typical feature of many C chondrites, which have up to 13 vol% refractory inclusions (e.g., Weisberg et al. [2006] and Table 1). In comparison, O chondrites generally contain less than 0.19 vol% refractory inclusions (Kimura et al. 2002). The abundances of such inclusions in R and E chondrites are much lower than that in Y-82094 (Table 1). The average size distribution of AOAs in Y-82094 is 290  $\mu\text{m}$  is within the range of CO chondrites, 150–440  $\mu\text{m}$  (Rubin 1998). The type distribution of CAIs, abundant type A and spinel-pyroxene inclusions, is typical of CO chondrites (Scott and Krot 2005). Having abundant porphyritic chondrules and rare nonporphyritic chondrules is a typical characteristic of most C chondrites (Table 2). The composition of the matrix is close to matrices in CO and CV chondrites, and different from that in the O chondrites (Fig. 9).

The bulk composition is similar to that of CO chondrites, and different from that of H chondrites, as mentioned above (Fig. 10). However, the volatile elements are evidently depleted, in comparison with other chondrites. We will discuss this unusual feature later. The oxygen isotopic composition of the whole rock is  $\delta^{17}\text{O} = -7.62\text{‰}$  and  $\delta^{18}\text{O} = -4.52\text{‰}$  (Yamaguchi et al. 2012). Thus, the oxygen isotope composition of Y-82094 is similar to that of CO and CV chondrites (Clayton and Mayeda 1999), although Y-82094 is relatively enriched in  $^{16}\text{O}$  compared with most CO and CV chondrites.

Based on bulk chemistry and oxygen isotopes, Y-82094 must be classified as a C chondrite. Kallemeyn and Wasson (1982) and Weisberg et al. (2006) suggested that CM-CO clan chondrites share the following

features: similar chondrule size distribution, similar refractory lithophile element abundance, and similar oxygen isotopic composition of high-temperature minerals. Some of these characteristic features of Y-82094, such as elemental abundance and oxygen composition, indicate that Y-82094, in part, resembles CM-CO clan chondrites. However, the chondrule size distribution, depletion of volatile elements, and modal abundance of components are unique characteristics of Y-82094 and distinguish it from the CM-CO clan. Silica minerals are rare in the mesostasis of C chondrite chondrule, although Acfer 094 contains them in its chondrules (Newton et al. 1995; Ushikubo et al. 2012), similar to those in Y-82094. Thus, the common occurrence of cristobalite in chondrules also characterizes Y-82094 and distinguishes it from most other C chondrites.

Type II chondrules are rare in Y-82094 (0.9%) in comparison with other C chondrites (5–10%) (Table 2). The abundance of Fe-Ni metal (8.1 vol%) is much higher than that of troilite (2.0 vol%), which is also a feature of Y-82094 that distinguishes it from CO and reduced CV chondrites. In the CO and reduced CV chondrites, sulfides (1.5–4.6 and 1.6–2.1 vol%) are comparable in abundance with the metal (1.3–5.9 and 1.1–4.6 vol%) (McSween 1977a, 1977b). They are unique features of this chondrite that distinguish it from the other C chondrites.

No similar C chondrite has been reported. The Meteoritical Bulletin database includes 35 ungrouped C chondrites as of September 2013. However, none of the previously reported ungrouped C chondrites have features similar to those of Y-82094. We observed all of the C chondrites, 199, presently in the NIPR collection (Japanese Collection of Antarctic Meteorite database), but did not find any similar to Y-82094. Therefore, we conclude that Y-82094 is an ungrouped (currently unique) C chondrite, having a set of characteristic features that are different from any known chondrite.

### Classification of Petrologic Type

Sharply defined chondrules, abundant clinoenstatite and apparent glass in chondrules, and the occurrence of opaque matrix are typical in type 3 chondrites. Sears et al. (1991) estimated that the petrologic type of Y-82094 is 3.5 by using TL data, although petrographical and mineralogical data to support this classification were not shown.

Next we discuss the petrologic subtype of Y-82094 from the observations obtained here. Kimura et al. (2008) proposed that the size and abundance of Ni-rich metal within kamacite grains in chondrules can be used to estimate petrologic type. According to their work, the

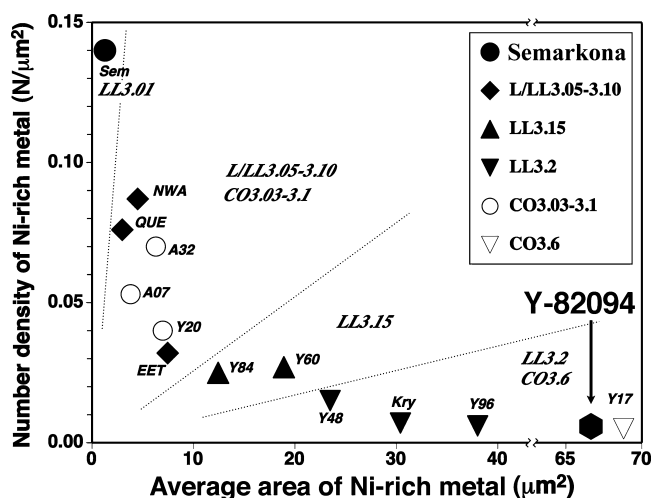


Fig. 11. Average area vs. number density diagram for Fe-Ni metal showing compositions of Ni-rich metal grains in Y-82094 chondrules, after the work of Kimura et al. (2008). On this diagram, Y-82094 metal plots within the range for type  $\geq 3.2$  chondrites.

grain size and number density of Ni-rich metal in kamacite increase and decrease with petrologic type, respectively, and can be used for petrologic classification of chondrites. Metals in Y-82094 chondrules show an intergrowth of fine-grained Ni-rich metal in kamacite (Fig. 7), which is similar to metals in type 3.2 O and CO chondrites (Kimura et al. 2008). Using the plot for number density versus average area of Ni-rich metals (from Kimura et al. 2008), Y-82094 metal plots in the area of type  $\geq 3.2$  (Fig. 11). Kamacite is enriched in Co, compared with Ni-rich metal. Fe-Ni metals in Y-82094 are depleted in Si, P, and Cr. All these observations are consistent with type  $\geq 3.2$  (Kimura et al. 2008). Shibata and Matsueda (1994) also suggested that this chondrite experienced weak thermal metamorphism, based on the occurrence of Ni-rich taenite.

The FeO-rich rims of AOA olivines are usually less than 3  $\mu\text{m}$  in width, indicative of type 3.2 (Chizmadia et al. 2002). Although type II chondrules are rare, the average  $\text{Cr}_2\text{O}_3$  content and standard deviation for FeO-bearing olivine grains are similar to values for the Kainsaz and Rainbow CO3.2 chondrites (Grossman and Brearley 2005). Melilite-rich inclusions decrease with increasing petrologic type (Rubin 1998; Russell et al. 1998), and the high abundance of melilite-rich CAIs in Y-82094 is consistent with that in CO 3.0–3.2 chondrites (Rubin 1998; Russell et al. 1998). From all of these data, we conclude that Y-82094 is petrologic type 3.2. This meteorite experienced weak thermal metamorphism, which is consistent with the sintered texture of the matrix, and the occurrences of weakly devitrified glass in chondrules.

## Formation Conditions

As mentioned above, Y-82094 shows unique features. These features cannot be explained by secondary processes, such as thermal metamorphism or impact on the parent body. The metamorphic and shock degrees are relatively low for this chondrite. Such weak secondary processes cannot explain the unusual size distribution of chondrules, and modal abundance of chondrules and matrix. We conclude that the unique features of this chondrite are primary, not the result of these secondary processes on the parent body.

One of the unique features of Y-82094 is the depletion in volatile elements in its bulk composition. Usually, such volatile elements are enriched in the matrix of C chondrites, relative to chondrules (Rubin and Wasson 1988; Bland et al. 2003; Huss et al. 2005). Therefore, the low abundance of the matrix in Y-82094 may be related to the depletion of volatile elements. The depletion of volatile elements, especially Rb, Cs, Pb, and Zn, suggests that Y-82094 considerably lacks the components condensed at temperatures  $< \sim 800$  K from a solar gas (e.g., Lodders 2003). The low abundance of troilite is consistent with this estimation.

The low abundance of type II chondrules is another unique feature of Y-82094. Dusty olivine and Ni-poor metal in chondrules, which are generally interpreted as evidence for reduction reactions, are not observed in Y-82094. Many type I chondrules in Y-82094 contain Fe-Ni metal spherules as mentioned above. However, these metals are not depleted in Ni, which is different from reduced Ni-poor metal (e.g., Rambaldi and Wasson 1982). Although the reverse zoning of silicates near secondary metal of reduction origin has been reported in chondrules (e.g., Kimura et al. 2003), it is not found in Y-82094. All of these observations exclude a secondary reduction origin for the high abundance of type I chondrules. Thus, the low abundance of type II chondrules is a primary feature resulting from chondrule formation in the nebular environment that formed the chondrules in Y-82094. Imae and Kojima (2000) suggested that the bulk FeO content is lower than that of other C chondrites, in spite of the similar content of total bulk Fe. This is consistent with the extremely low abundance of type II chondrules and high abundance of Fe-Ni metal in type I chondrules, as described above. We conclude that most chondrules in Y-82094 formed under reducing conditions, and accreted to the parent body. Such a formation process, along with unique petrologic and chemical features of Y-82094, suggests different formation condition from other C chondrites. We suggest that the range of formation conditions for C chondrites is wider than currently recorded by the major C chondrite groups.

## CONCLUSIONS

Y-82094 is classified as an unusual chondrite of type 3.2. It has a combination of features that distinguish it from any other known chondrite. Its high chondrule:matrix ratio is similar to O chondrites. However, the bulk composition, abundant refractory inclusions, and oxygen isotopic composition are typical of C chondrites. No similar C chondrite has been reported. Nevertheless, we predict that more Y-82094-like chondrites will be found, possibly among chondrites previously classified as “CO” and from future meteorite recoveries.

The constituent components of Y-82094 formed under high-temperature and reducing conditions, in comparison with the other C chondrites. Y-82094 may represent a new, previously unsampled, asteroidal body. Ungrouped C chondrites, such as Y-82094, suggest a wider range of chondrite parent bodies and formation conditions than currently recorded by the major C chondrite groups. Discovery of new meteorites such as Y-82094 stresses the importance of continued expeditions to Antarctica, as well as other locations, to recover new types of meteorites that expand our sampling of solar system materials.

*Acknowledgments*—The sections were loaned from the NIPR. Denton Ebel is thanked for help in X-ray mapping of section 111-1. We appreciate the careful reviews by A. Bischoff and A. E. Rubin. We also thank the associate editor M. E. Zolensky for efficient handling of the manuscript. This work was supported by a Grant-in-aids of Ministry of Education, Science, Sport, and Culture of Japanese government, No. 22540488 to M. K. and NASA Grant NNX12AI06G to M. K. W.

*Editorial Handling*—Dr. Michael Zolensky

## REFERENCES

- Barrat J. A., Zanda B., Moynier F., Bollinger C., Liorzou C., and Bayon G. 2012. Geochemistry of CI chondrites: Major and trace elements, and Cu and Zn isotopes. *Geochimica et Cosmochimica Acta* 83:79–92.
- Bischoff A., Vogel N., and Roszjar J. 2011. The Rumuruti chondrite group. *Chemie der Erde* 71:101–133.
- Bland P. A., Alard O., Gounelle M., and Rogers N. W. 2003. Trace element variation in carbonaceous chondrite matrix (abstract #1750). 34th Lunar and Planetary Science Conference. CD-ROM.
- Brearley A. J. and Jones R. H. 1998. Chondritic meteorites. In *Planetary materials*, edited by Papike J. J., Washington, D.C.: Mineralogical Society of America. pp. 3-1–3-398.
- Chizmadia L. J., Rubin A. E., and Wasson J. T. 2002. Mineralogy and petrology of amoeboid olivine inclusions in CO3 chondrites: Relationship to parent-body aqueous alteration. *Meteoritics & Planetary Science* 37:1781–1796.
- Clayton R. N. and Mayeda T. K. 1999. Oxygen isotope studies of carbonaceous chondrites. *Geochimica et Cosmochimica Acta* 63:2089–2104.
- Grossman J. N. and Brearley A. J. 2005. The onset of metamorphism in ordinary and carbonaceous chondrites. *Meteoritics & Planetary Science* 40:87–122.
- Huss G. R., Keil K., and Taylor G. J. 1981. The matrices of unequilibrated ordinary chondrites: Implications for the origin and history of chondrites. *Geochimica et Cosmochimica Acta* 45:33–51.
- Huss G. R., Alexander C. M. O'D., Palme H., Bland P. A., and Wasson J. T. 2005. Genetic relationships between chondrules, fine-grained rims, and interchondrule matrix. In *Chondrites and the protoplanetary disk*, vol. 341, edited by Krot A. N., Scott E. R. D., and Reipurth B. Tucson, Arizona: The University of Arizona Press. pp. 701–731.
- Ikeda Y., Kimura M., Mori H., and Takeda H. 1981. Chemical compositions of matrices of unequilibrated ordinary chondrites. *Memoir of National Institute of Polar Research, Special Issue* 20:124–144.
- Imae N. and Kojima H. 2000. Sulfide textures of a unique CO3-chondrite (Y-82094) and its petrogenesis. *Antarctic Meteorite Research* 13:55–64.
- Jones R. H. 2012. Petrographic constraints on the diversity of chondrule reservoirs in the protoplanetary disk. *Meteoritics & Planetary Science* 47:1176–1190.
- Kallemeyn G. W. and Wasson J. T. 1982. The compositional classification of chondrites: III. Ungrouped carbonaceous chondrites. *Geochimica et Cosmochimica Acta* 46:2217–2228.
- Kimura M., Hiyagon H., Palme H., Spettel B., Wolf D., Clayton R. N., Mayeda T. K., Sato T., Suzuki A., and Kojima H. 2002. The most primitive H-chondrites: Y792947, Y793408 and Y82038, with abundant refractory inclusions. *Meteoritics & Planetary Science* 37:1417–1434.
- Kimura M., Hiyagon H., Lin Y., and Weisberg M. K. 2003. FeO-rich silicates in the Sahara 97159 (EH3) enstatite chondrite: Mineralogy, oxygen isotopic compositions, and origin. *Meteoritics & Planetary Science* 38:389–398.
- Kimura M., Nakajima H., Hiyagon H., and Weisberg M. K. 2006. Spinel group minerals in LL3.00-6 chondrites: Indicators of nebular and parent body processes. *Geochimica et Cosmochimica Acta* 70:5634–5650.
- Kimura M., Grossman J. N., and Weisberg M. K. 2008. Fe-Ni metal in primitive chondrites: Indicators of classification and metamorphic conditions for ordinary and CO chondrites. *Meteoritics & Planetary Science* 43:1161–1177.
- Kimura M., Barrat J. A., Weisberg M. K., Imae N., Yamaguchi A., and Kojima H. 2012. Ungrouped carbonaceous chondrite, Yamato 82094: Characteristic features and classification (abstract). *Meteoritics & Planetary Science* 47:5084.pdf.
- Krot A. N., Petaev M. I., and Yurimoto H. 2004. Amoeboid olivine aggregates with low-Ca pyroxenes: A genetic link between refractory inclusions and chondrules? *Geochimica et Cosmochimica Acta* 68:1923–1941.
- Lodders K. 2003. Solar system abundances and condensation temperatures of the elements. *The Astrophysical Journal* 591:1220–1247.

- McSween H. Y. Jr. 1977a. Carbonaceous chondrites of the Ornans type: A metamorphic sequence. *Geochimica et Cosmochimica Acta* 41:477–491.
- McSween H. Y. Jr. 1977b. Petrographic variations among carbonaceous chondrites of the Vigarano type. *Geochimica et Cosmochimica Acta* 41:1777–1790.
- Newton J., Bischoff A., Arden J. W., Franchi I. A., Geiger T., Greshake A., and Pillinger C. T. 1995. Acfer 094, a uniquely primitive carbonaceous chondrite from the Sahara. *Meteoritics* 30:47–56.
- Rambaldi E. R. and Wasson J. T. 1982. Fine, nickel-poor Fe-Ni grains in the olivine of unequilibrated ordinary chondrites. *Geochimica et Cosmochimica Acta* 46:929–939.
- Rubin A. E. 1989. Size-frequency distributions of chondrules in CO3 chondrites. *Meteoritics* 24:179–189.
- Rubin A. E. 1998. Correlated petrologic and geochemical characteristics of CO3 chondrites. *Meteoritics & Planetary Science* 33:385–391.
- Rubin A. E. 2010. Physical properties of chondrules in different chondrite groups: Implications for multiple melting events in dusty environments. *Geochimica et Cosmochimica Acta* 74:4807–4828.
- Rubin A. E. and Wasson J. T. 1988. Chondrules and matrix in the Ornans CO3 meteorite: Possible precursor components. *Geochimica et Cosmochimica Acta* 52:425–432.
- Russell S. S., Huss G. R., Fahey A. J., Greenwood R. C., Hutchison R., and Wasserburg G. J. 1998. An isotopic and petrologic study of calcium-aluminum-rich inclusions from CO3 meteorites. *Geochimica et Cosmochimica Acta* 62:689–714.
- Scott E. R. D. and Krot A. N. 2005. Chondrites and their components. In *Meteorites, comets, and planets*, edited by Davis A. M. Treatise on Geochemistry, vol. 1. Amsterdam: Elsevier. pp. 143–200.
- Scott E. R. D., Keil K., and Stöffler D. 1992. Shock metamorphism of carbonaceous chondrites. *Geochimica et Cosmochimica Acta* 56:4281–4293.
- Sears D. W. G., Batchelor J. D., Lu J., and Keck B. D. 1991. Metamorphism of CO and CO-like chondrites and comparisons with type 3 ordinary chondrites. *Proceeding of the NIPR Symposium of Antarctic Meteorites* 4:319–343.
- Shibata Y. and Matsueda H. 1994. Chemical composition of Fe-Ni metal and phosphate minerals in Yamato-82094 carbonaceous chondrite. *Proceeding of the NIPR Symposium of Antarctic Meteorites* 7:110–124.
- Ushikubo T., Kimura M., Kita N. T., and Valley J. W. 2012. Primordial oxygen isotope reservoirs of the solar nebula recorded in chondrules in Acfer 094 carbonaceous chondrite. *Geochimica et Cosmochimica Acta* 90:242–264.
- Wasson J. T. and Kallemeyn G. W. 1988. Compositions of chondrites. *Philosophical Transaction of Royal Society in London A* 325:535–544.
- Weisberg M. K., McCoy T. J., and Krot A. N. 2006. Systematics and evaluation of meteorite classification. In *Meteorites and the early solar system II*, edited by Lauretta D. S. and McSween H. Y. Jr. Tucson, Arizona: The University of Arizona Press. pp. 19–52.
- Weisberg M. K., Ebel D. S., Connolly H. C. Jr., Kita N. T., and Ushikubo T. 2011. Petrology and oxygen isotope compositions of chondrules in E3 chondrites. *Geochimica et Cosmochimica Acta* 75:6556–6569.
- Yamaguchi A., Barrat J.-A., Ito M., and Bohn M. 2011. Post-ecritic magmatism on Vesta: Evidence from the petrology and thermal history of diogenites. *Journal of Geophysical Research* 116:E08009.
- Yamaguchi A., Imae N., Kimura M., and Kojima H. 2012. *Meteorite Newsletter*, vol. 21. Tokyo: NIPR.
- Yanai K. and Kojima H. 1987. *Petrographic catalog of the Antarctic meteorites*. Tokyo: NIPR.
- Zolensky M., Barrett R., and Browning L. 1993. Mineralogy and composition of matrix and chondrule rims in carbonaceous chondrites. *Geochimica et Cosmochimica Acta* 57:3123–3148.
-